



Signaling and Immunoresolving Actions of Resolvin D1 in Inflamed Human Visceral Adipose Tissue

This information is current as
of February 26, 2022.

Esther Titos, Bibiana Rius, Cristina López-Vicario, José Alcaraz-Quiles, Verónica García-Alonso, Aritz Lopategi, Jesmond Dalli, Juan José Lozano, Vicente Arroyo, Salvadora Delgado, Charles N. Serhan and Joan Clària

J Immunol 2016; 197:3360-3370; Prepublished online 19
September 2016;

doi: 10.4049/jimmunol.1502522

<http://www.jimmunol.org/content/197/8/3360>

Supplementary Material <http://www.jimmunol.org/content/suppl/2016/09/17/jimmunol.1502522.DCSupplemental>

References This article **cites 34 articles**, 11 of which you can access for free at:
<http://www.jimmunol.org/content/197/8/3360.full#ref-list-1>

Why *The JI*? Submit online.

- **Rapid Reviews! 30 days*** from submission to initial decision
- **No Triage!** Every submission reviewed by practicing scientists
- **Fast Publication!** 4 weeks from acceptance to publication

**average*

Subscription Information about subscribing to *The Journal of Immunology* is online at:
<http://jimmunol.org/subscription>

Permissions Submit copyright permission requests at:
<http://www.aai.org/About/Publications/JI/copyright.html>

Email Alerts Receive free email-alerts when new articles cite this article. Sign up at:
<http://jimmunol.org/alerts>

Signaling and Immunoresolving Actions of Resolvin D1 in Inflamed Human Visceral Adipose Tissue

Esther Titos,^{*,†} Bibiana Rius,^{*} Cristina López-Vicario,^{*} José Alcaraz-Quiles,^{*} Verónica García-Alonso,^{*} Aritz Lopategi,^{*} Jesmond Dalli,[‡] Juan José Lozano,[†] Vicente Arroyo,[§] Salvadora Delgado,[¶] Charles N. Serhan,[‡] and Joan Clària^{*,†,||}

Persistent activation of the innate immune system greatly influences the risk for developing metabolic complications associated with obesity. In this study, we explored the therapeutic potential of the specialized proresolving mediator (SPM) resolvin D1 (RvD1) to actively promote the resolution of inflammation in human visceral adipose tissue from obese (Ob) patients. Using liquid chromatography–tandem mass spectrometry–based metabololipidomic analysis, we identified unbalanced production of SPMs (i.e., D- and E-series resolvins, protectin D1, maresin 1, and lipoxins) with respect to inflammatory lipid mediators (i.e., leukotriene B₄ and PGs) in omental adipose tissue from Ob patients. In parallel, high-throughput transcriptomic analysis revealed a unique signature in this tissue that was characterized by overactivation of the IL-10 signaling pathway. Incubation of inflamed Ob visceral adipose tissues and human macrophages with RvD1 limited excessive activation of the IL-10 pathway by reducing phosphorylation of STAT proteins. Of interest, RvD1 blocked STAT-1 and its target inflammatory genes (i.e., CXCL9), as well as persistent STAT3 activation, without affecting the IL-10 anti-inflammatory response characterized by inhibition of IL-6, IL-1 β , IL-8, and TNF- α . Furthermore, RvD1 promoted resolution by enhancing expression of the IL-10 target gene heme oxygenase-1 by mechanisms dependent on p38 MAPK activity. Together, our data show that RvD1 can tailor the quantitative and qualitative responses of human inflamed adipose tissue to IL-10 and provide a mechanistic basis for the immunoresolving actions of RvD1 in this tissue. These findings may have potential therapeutic implications in obesity-related insulin resistance and other metabolic complications. *The Journal of Immunology*, 2016, 197: 3360–3370.

A chronic state of low-grade inflammation in adipose tissue is recognized as a critical factor for the progression of metabolic complications associated with obesity, such as insulin resistance and nonalcoholic fatty liver disease (NAFLD) (1, 2). Indeed, these obesity-related comorbidities are closely linked to the presence of persistent activation of proinflammatory signaling pathways in adipose tissue, which severely disrupts key metabolic checkpoints in this tissue (1, 2). Among these signals, enhanced production of proinflammatory adipokines, such as TNF- α , IL-6, IL-1 β , MCP-1, leptin, and resistin, accompanied by a reduction in the anti-inflammatory adipokine, adiponectin, are common findings in obese (Ob) individuals with metabolic syndrome (3, 4).

In addition to the heightened production of inflammatory mediators, Ob adipose tissue shows an intrinsic inability to resolve uncontrolled inflammation and to restore tissue homeostasis and

functionality (5). Current evidence indicates that inflammation does not switch off in a passive manner but involves a program of unique endogenous mechanisms and mediators that orchestrate its active resolution in a timely and effective manner (6). Among these, lipid mediators, such as lipoxins, resolvins, protectins, and maresins, collectively known as specialized proresolving mediators (SPMs), have attracted the most attention (7). SPMs act as braking signals for the persistent vicious cycle leading to unremitting inflammation and primarily as promoters of active resolution of inflammation. Indeed, at the preclinical level, therapeutic administration of SPMs promotes resolution of inflamed adipose tissue and protects mice against obesity-associated complications, such as insulin resistance and NAFLD (8–12). An interesting aspect of these mediators is that they are able to take advantage of macrophage plasticity by inducing changes in the phenotype of

^{*}Department of Biochemistry and Molecular Genetics, Hospital Clínic, August Pi i Sunyer Biomedical Research Institute, Barcelona 08036, Spain; [†]Biomedical Research Networking Center on Liver and Digestive Diseases, Barcelona 08036, Spain; [‡]Department of Anesthesiology, Perioperative and Pain Medicine, Center for Experimental Therapeutics and Reperfusion Injury, Brigham and Women's Hospital and Harvard Medical School, Boston, MA 02115; [§]European Foundation for the Study of Chronic Liver Failure, Barcelona 08036, Spain; [¶]Department of Gastrointestinal Surgery, Hospital Clínic, August Pi i Sunyer Biomedical Research Institute, Barcelona 08036, Spain; and ^{||}Department of Biomedical Sciences, University of Barcelona, Barcelona 08036, Spain

ORCIDs: 0000-0002-2543-2243 (E.T.); 0000-0003-4627-8545 (C.N.S.); 0000-0003-4333-7749 (J.C.).

Received for publication December 2, 2015. Accepted for publication August 22, 2016.

This work was supported by the Ministry of Economy and Competitiveness (Grants SAF12/32789, SAF15-63674-R, and PIE14/00045) under European Regional Development Funds (to J.C.) and in part by National Institutes of Health Grant P01GM095467 (to C.N.S.). The Biomedical Research Networking Center on Liver and Digestive Diseases is funded by the Instituto de Salud Carlos III. This study was carried out at the Center Esther Koplowitz. C.L.-V. was supported by the

August Pi i Sunyer Biomedical Research Institute/Fundació Clínic. V.G.-A. and B.R. have fellowships from the Ministry of Economy and Competitiveness. A.L. was funded by a Marie Curie Action, and J.A.-Q. is a recipient of an Agaur fellowship (FI-DGR 2015).

The microarray data presented in this article have been submitted to the Gene Expression Omnibus under accession number GSE71415.

Address correspondence and reprint requests to Dr. Esther Titos and Dr. Joan Clària, Department of Biochemistry and Molecular Genetics, Hospital Clínic, Villarroel 170, Barcelona 08036, Spain. E-mail addresses: esther.titos@ciberehd.org (E.T.) and jclaria@clinic.ub.es (J.C.)

The online version of this article contains supplemental material.

Abbreviations used in this article: ADP, adipocyte; BMI, body mass index; CT, control; DPBS, Dulbecco's PBS; FAF, fatty acid free; HO, heme oxygenase; IL-1ra, IL-1 β receptor antagonist; LC-MS/MS, liquid chromatography–tandem mass spectrometry; LT, leukotriene; LX, lipoxin; NAFLD, nonalcoholic fatty liver disease; Ob, obese; PLS-DA, partial least squares–discriminant analysis; pSTAT3^{Tyr}, Tyr⁷⁰⁵ phosphorylation of STAT3; RvD1, resolvin D1; SOCS, suppressor of cytokine signaling; SPM, specialized proresolving mediator; SVC, stromal vascular cell.

Copyright © 2016 by The American Association of Immunologists, Inc. 0022-1767/16/\$30.00

recruited adipose tissue macrophages toward a proresolution M2 state (8, 10). In addition, SPMs enhance the emergence of pro-resolving macrophages expressing low levels of CD11b and producing the anti-inflammatory cytokine IL-10 (13). Moreover, SPMs induce monocyte differentiation into phagocytosing macrophages, facilitating the removal of dead or dying cells (efferocytosis) and enhancing phagocyte efflux to drain lymph nodes to aid in clearing out the inflamed tissues (14, 15). All of these processes positively contribute to the resolution of adipose tissue inflammation and the prevention of metabolic syndrome in obesity.

The present study was undertaken to advance the concept of resolution as an active phenomenon aimed at suppressing uncontrolled inflammation in human Ob adipose tissue. This study had three main objectives: to translate the findings obtained in preclinical models to real-world human samples of adipose tissue from Ob individuals; to characterize the intracellular signaling pathways by which SPMs may exert proresolving actions in inflamed adipose tissue in a series of mechanistic studies in human adipose tissue and macrophages; and to provide proof of concept that targeting SPM signaling pathways is worthy of further investigation. Through experiments with the representative SPM

resolvin D1 (RvD1), we provide evidence that SPMs promote proresolving responses in inflamed human adipose tissue by interacting with the signaling pathways of IL-10 and by modulating the archetypal anti-inflammatory response of this cytokine.

Materials and Methods

Study participants and sample collection

Forty-one individuals with obesity undergoing laparoscopic bariatric surgery and seven patients without a history of obesity undergoing laparoscopic cholecystectomy were recruited from the Gastroenterology Surgery Unit of the Hospital Clínic of Barcelona and included in the study. Participants were selected according to their body mass index (BMI), calculated as mass/height², and categorized as nonobese controls (CTs) (BMI < 29.9 kg/m², *n* = 7) and Ob (BMI > 29.9 kg/m², *n* = 41). Individuals with inflammatory bowel disease or cancer and Ob patients with previous bariatric surgery were excluded from the study. Harvested omental adipose tissue samples were washed twice with Dulbecco's PBS (DPBS) and minced into ≈100-mg pieces, placed in 10% formalin or snap-frozen in liquid nitrogen, and stored at -80°C for further analysis. Demographic data, clinical data, and drug use were collected from patients' electronic medical records. All studies were conducted in accordance with the criteria of the Investigation and Ethics Committee of the Hospital Clínic, and written informed consent was obtained from all participants (protocol #2012-7239).

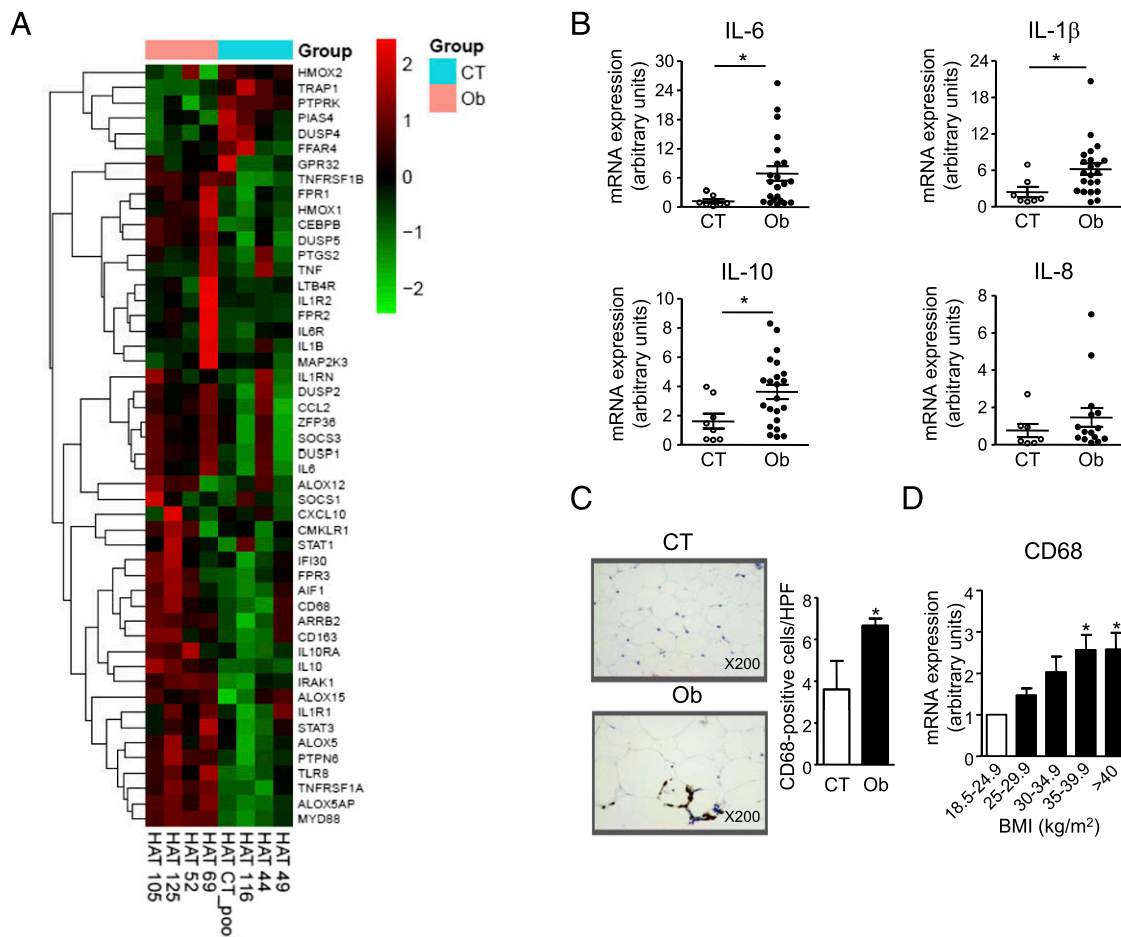


FIGURE 1. High-throughput transcriptome analysis of human Ob visceral adipose tissue. **(A)** Upregulated expression of inflammation-related genes (Affymetrix Human Genome U219 expression array plate) in visceral adipose tissue from Ob and nonobese CT subjects. Results are expressed as a matrix view of gene-expression data (heat map) where rows represent genes and columns represent hybridized samples. The intensity of each color denotes the standardized ratio between each value and the average expression of each gene across all samples. Red pixels correspond to an increased abundance of mRNA in the human adipose tissue samples indicated, whereas green pixels indicate decreased mRNA levels. **(B)** Relative mRNA levels for IL-6, IL-1β, IL-10, and IL-8 in human adipose tissue from CT (*n* = 8) and Ob (*n* = 22) subjects were assessed by real-time PCR. **(C)** Representative photomicrographs of adipose tissue sections stained with the macrophage marker CD68 in CT (BMI < 29.9) and Ob (BMI > 29.9) individuals (original magnification ×200) (left panels). Number of CD68⁺ cells/high-power field in human adipose tissue sections from CT (*n* = 3) and Ob (*n* = 10) subjects (right panel). **(D)** Adipose tissue CD68 gene expression in relation to BMI (*n* = 20) was analyzed by real-time PCR. Pooled human adipose tissue RNA from 18 healthy subjects served as a calibrator. Data are mean ± SEM. **p* < 0.05 versus CT subjects.

Biochemical analyses

Serum concentrations of glucose, cholesterol, triglyceride, alanine aminotransferase, and aspartate aminotransferase were determined by standard laboratory procedures.

Immunohistochemistry analysis

The tissues were routinely fixed in 10% buffered formalin, embedded in paraffin, and sectioned into 2- μ m-thick sections for CD68 immunohistochemistry with FLEX Ready-to-Use monoclonal mouse anti-human CD68

Ab (Dako) and H&E counterstain at the Pathology Department of the Hospital Clínic. For quantitative analysis, the number of CD68⁺ cells was counted in 15 high-power fields/tissue section under a light microscope (Eclipse E600 microscope; Nikon) at 400 \times magnification, and results are given as the number of positive cells/high-power field.

Adipose tissue explants and ex vivo incubations

Human visceral adipose tissue from Ob patients was collected under sterile conditions and placed in a P100 plate with prewarmed (37°C) DPBS containing antibiotics (penicillin [100 U/ml] and streptomycin [100 μ g/ml]).

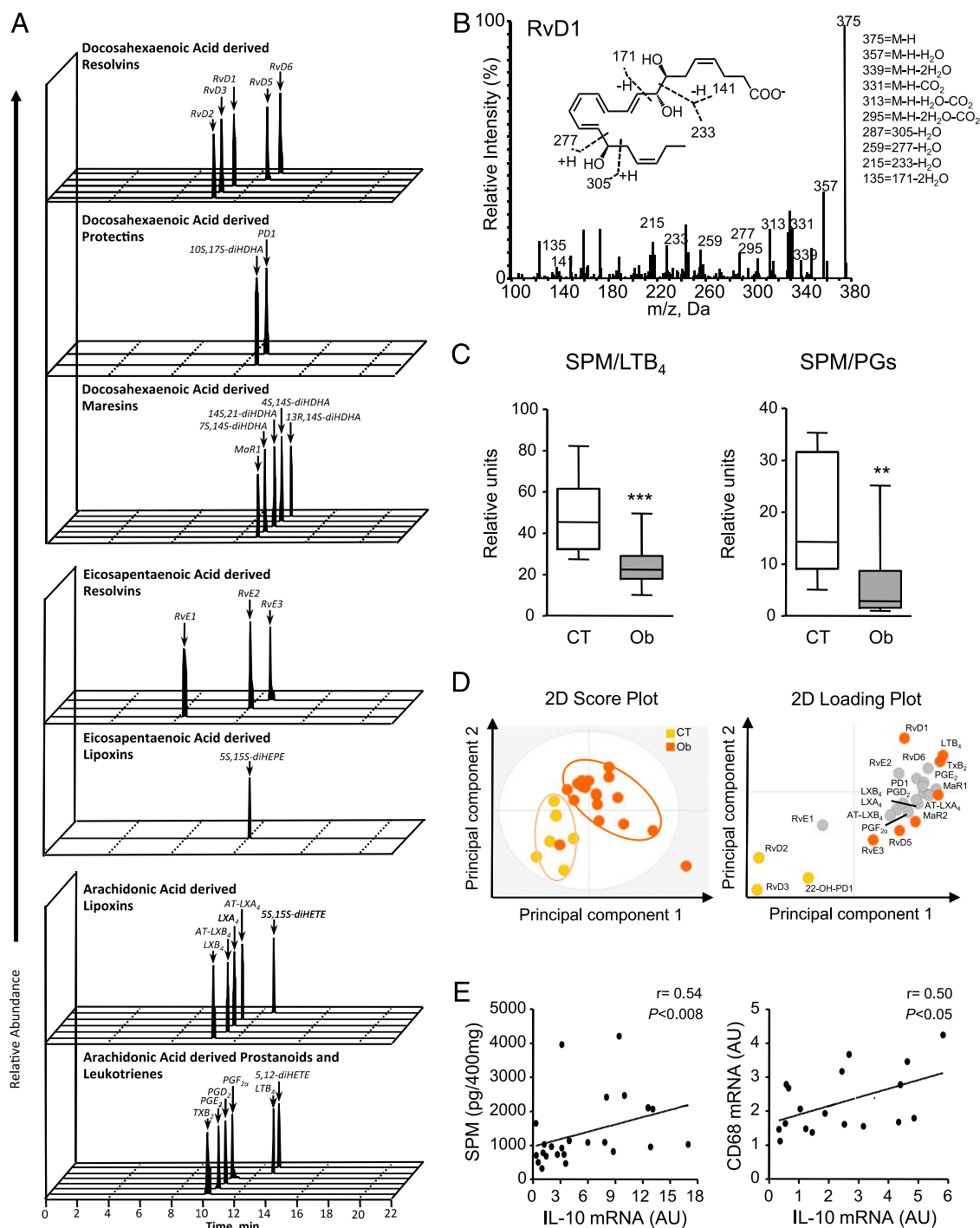


FIGURE 2. Distinct lipid mediator-SPM signature profiles in visceral adipose tissues from Ob and nonobese patients. **(A)** Representative multiple reaction monitoring chromatograms obtained by liquid chromatography–tandem mass spectrometry (LC-MS/MS)-based metabololipidomics of selected ion pairs for docosahexaenoic acid-, eicosapentaenoic acid-, and arachidonic acid-derived lipid mediators. Results are representative of $n = 24$ adipose tissue samples. **(B)** Tandem mass spectra used in the identification of RvD1. **(C)** SPM/LTB₄ (including its all-*trans* isomer) and SPM/PG ratios in human adipose tissue from CT ($n = 6$) and Ob ($n = 18$) individuals. **(D)** PLS-DA of lipid mediator profiles from Ob and nonobese adipose tissue. **(E)** Correlations (Spearman's rho test) between SPM and IL-10 (left panel) and between CD68 and IL-10 (right panel) in human visceral adipose tissue. Data are mean \pm SEM. ** $p < 0.005$, *** $p < 0.001$ versus CT subjects.

Connective tissue and blood vessels were removed by dissection before cutting the tissue into small pieces (60–80 mg). Explants were washed with DPBS at 37°C by centrifugation for 1 min at 400 × *g* to remove blood cells and then maintained overnight in culture in DMEM with L-glutamine (2 mM), antibiotics, and 10% FBS. After a gentle rinse in DPBS containing penicillin and streptomycin, treatments were performed in DMEM with L-glutamine, antibiotics, and 1% endotoxin-free BSA–fatty acid free (FAF) (Sigma). Protein and mRNA expression was assessed in explants incubated with vehicle (0.01% EtOH) or RvD1 (1, 10, and 50 nM) (Cayman Chemicals) for 30 min, followed by the addition of cytokines (IL-10 [20 ng/ml], IL-1β [25 pg/ml], and IL-6 [10 ng/ml]) (R&D Systems) for 0.5, 2, and 6 h at 37°C. For experiments assessing IL-10 production, adipose tissue was incubated with 5 μM SB203580 (p38 MAPK inhibitor XVI; Merck Millipore) in the presence of RvD1 (1, 10, and 50 nM) for 30 min before the addition of LPS (1 μg/ml) (Sigma) for 24 h. At the end of the incubation periods, supernatants were collected, and explants were frozen in liquid nitrogen, placed in polypropylene tubes, and stored at –80°C for further analysis.

Isolation of adipocytes and stromal vascular cells

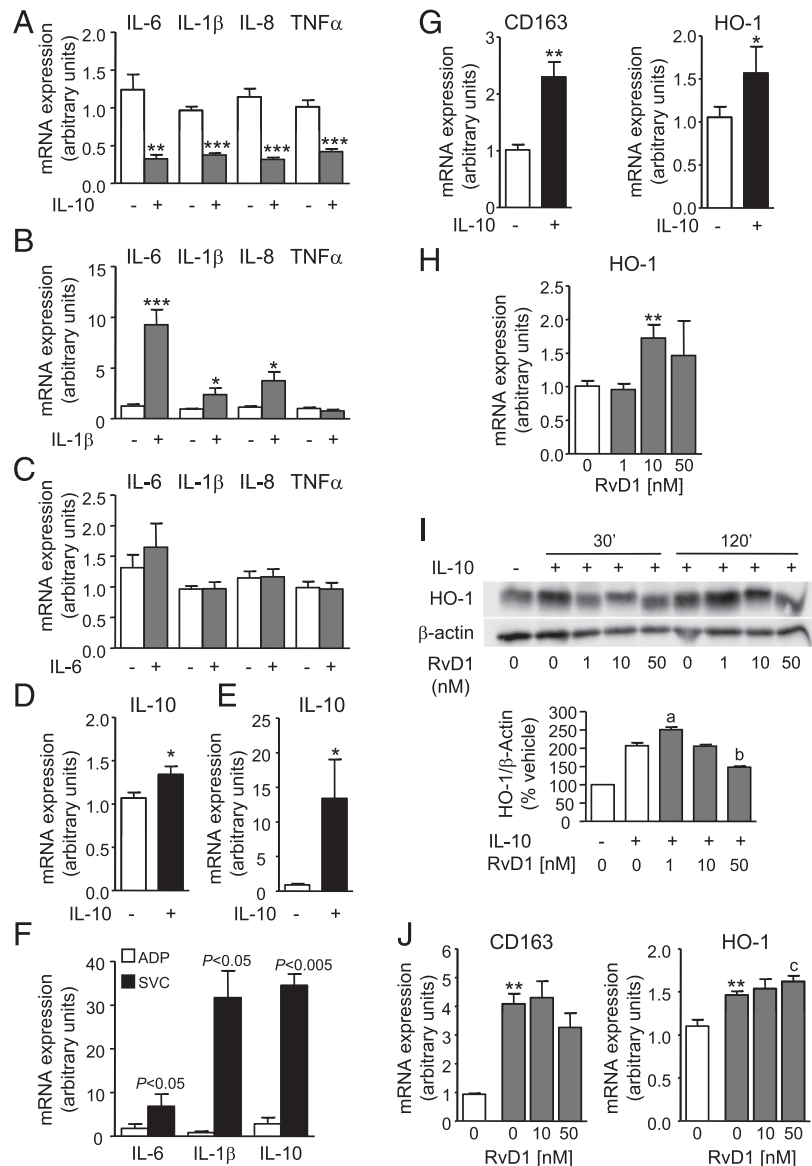
Adipose tissue samples (3–7 g) were washed extensively with sterile DPBS containing antibiotics to remove contaminating blood cells. Then the specimens were carefully cut into 0.6–1.0-g pieces, avoiding connective tissue and blood vessels. Explants were washed with DPBS at 37°C by centrifugation for 1 min at 400 × *g* to remove blood cells. Tissue was finely minced, placed in 5 ml of digestion buffer containing Krebs Ringer supplemented with 1.5% BSA-FAF and 2.5 mg/ml of Liberase (Roche

Diagnostics), and incubated at 37°C for 45 min with gentle shaking. Tissue homogenates were filtered through a 100-μm nylon mesh and maintained in Krebs Ringer buffer supplemented with 1.5% BSA-FAF and 2 mM EDTA for 10 min. Floating cells (adipocytes [ADPs]) were collected, homogenized in 1 ml of TRIzol reagent (Invitrogen), and stored at –80°C for further analysis. The infranatant containing the stromal vascular cells (SVCs) was centrifuged at 500 × *g* for 5 min; pelleted cells were homogenized in 1 ml of TRIzol reagent and kept at –80°C until further analysis.

Cell culture and cell incubations

The human monocyte cell line THP-1 (American Type Culture Collection, Manassas, VA) was cultured in RPMI 1640 medium containing 10% FBS and antibiotics at 37°C in a 5% CO₂ incubator. Before performing the experiments, the growth medium was exchanged for serum-free RPMI 1640 medium for 18 h. In some experiments, unstimulated THP-1 cells or THP-1 cells differentiated into macrophage-like cells by the addition of PMA (50 ng/ml; Sigma) for 48 h were seeded (8×10^5 – 1×10^6) into 12- and 24-well plates and incubated at 37°C in serum-free RPMI 1640 medium in the presence of vehicle (0.01% EtOH) and RvD1 (1, 10 and 50 nM) for 30 min, followed by the addition of increasing concentrations of IL-10 (2, 20, 100, and 200 ng/ml), IL-6 (0.05, 10, and 20 ng/ml), and IL-1β (25 pg/ml) for 10 min. Specifically, for IL-10–treated cells, an additional 6 h time point was performed. For experiments assessing suppressor of cytokine signaling (SOCS)3 stabilization, THP-1 cells were incubated or not with IL-10 (20 ng/ml) for 30 min before the addition of IL-6 (10 ng/ml) in the presence or absence of 10 μM of the proteasome inhibitor MG132

FIGURE 3. RvD1 potentiates IL-10–induced HO-1 expression in human Ob adipose tissue and macrophages. **(A)** Relative mRNA levels for IL-6, IL-1β, IL-8, and TNF-α in Ob adipose tissue explants incubated for 6 h in the absence (–) or presence (+) of IL-10 (20 ng/ml). **(B)** Changes in gene expression in response to IL-1β (25 pg/ml). **(C)** Changes in gene expression in response to IL-6 (10 ng/ml). **(D)** Changes in IL-10 mRNA expression in Ob adipose tissue explants incubated with IL-10 (20 ng/ml). **(E)** mRNA expression of IL-10 in THP-1–derived macrophages incubated with IL-10 (20 ng/ml) for 6 h. **(F)** mRNA expression of IL-6, IL-1β, and IL-10 was analyzed in ADPs and SVCs isolated from human Ob adipose tissue. **(G)** Relative mRNA expression for the anti-inflammatory genes CD163 and HO-1 in Ob adipose tissue explants incubated for 6 h in the absence (–) or presence (+) of IL-10 (20 ng/ml). **(H)** Changes in HO-1 mRNA expression in response to increasing concentrations of RvD1 (0, 1, 10, and 50 nM). **(I)** Representative immunoblot of HO-1 protein expression assessed by Western blot in Ob adipose tissue explants in the presence of increasing concentrations of RvD1 (0, 1, 10, and 50 nM) for 30 min, followed by addition of IL-10 (20 ng/ml) for 30 or 120 min (upper panel). **(J)** Relative mRNA expression for the anti-inflammatory genes CD163 and HO-1 in Ob adipose tissue explants incubated in the presence of increasing concentrations of RvD1 (0, 1, 10 and 50 nM) for 30 min followed by addition of IL-10 (20 ng/ml) for 6 h. Densitometric analysis at 120 min (lower panel). Data are mean ± SEM of *n* = 3 independent experiments performed in duplicate. **p* < 0.05, ***p* < 0.005, ****p* < 0.0005 versus nontreated adipose tissue explants. ^a*p* < 0.05, ^b*p* < 0.005, RvD1- versus IL-10–treated explants at time 120 min. ^c*p* < 0.05 versus IL-10–treated cells.



(Calbiochem, Merck Millipore) for 5 h. To verify the effects of MG132 in preventing the proteolytic degradation of newly synthesized SOCS3 by the ubiquitin-proteasome system (16), additional experiments were performed in THP-1 cells incubated in the absence or presence of MG132 (10 μ M) for 30 min before the addition of IL-6 (10 ng/ml) for 5 h. In some experiments, LPS stimulation was performed in the presence of a mouse monoclonal anti-human IL-10R (10 μ g/ml) or CT nonimmune mouse IgG (R&D Systems). At the end of the incubation periods, cells and supernatants were collected for further analysis.

RNA isolation, reverse-transcription, and real-time PCR

Isolation of total RNA from adipose tissue, ADPs, SVCs, and THP-1 cells was performed using TRIzol reagent. RNA concentration was assessed in a NanoDrop 1000 spectrophotometer (NanoDrop Technologies), and its integrity was tested with an RNA 6000 Nano Assay in a Bioanalyzer 2100 (Agilent Technologies). cDNA synthesis from 0.5 to 1 μ g of total RNA was performed using the High-Capacity cDNA Archive Kit (Applied Biosystems). Real-time PCR analysis of SOCS1 (Hs00705164_s), SOCS3 (Hs02330328_s1), IL-1 β (Hs01555410_m1), IL-8 (Hs00174103_m1), IL-6 (Hs00985639_m1), IL-6 signal transducer (Hs00174360_m1), IL-6R α (Hs01075666_m1), cyclooxygenase-2 (Hs00153133_m1), TNF- α (Hs01113624_g1), IL-10 (Hs00961622_m1), CD163 (Hs00174705_m1), heme oxygenase (HO)-1 (Hs01110250_m1), HO-2 (Hs01558390_m1), CXCL9 (Hs00171065_m1), and CXCL10 (Hs01124251_g1) was performed in a 7900HT Fast System (Applied Biosystems) using β -actin (Hs99999903_m1) as the endogenous CT. PCR results were analyzed with Sequence Detector 2.1 software (Applied Biosystems). Relative quantification of gene expression was performed using the comparative Ct method. The amount of target gene, normalized to β -actin and relative to a calibrator, was determined by the arithmetic equation $2^{-\Delta\Delta C_t}$, as described in the comparative Ct method (<http://docs.appliedbiosystems.com/pebi/docs/04303859.pdf>). For analysis of real-time PCR data from patients, total RNA derived from normal human adipose tissue pooled from 18 individuals (Clontech Laboratories) was used as a calibrator.

Western blot analysis

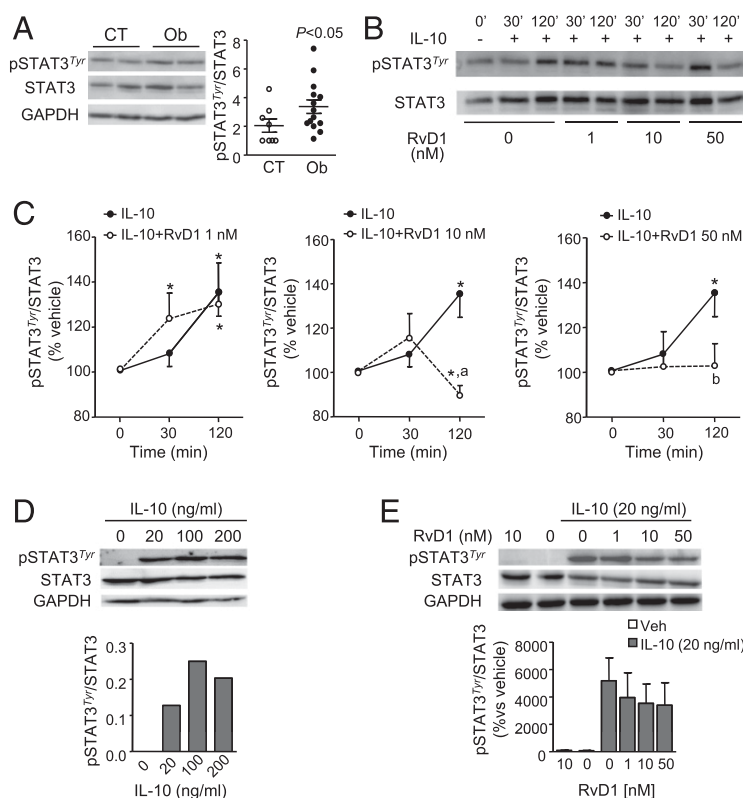
Total protein was extracted using lysis buffer containing 50 mM HEPES, 20 mM β -glycerophosphate, 2 mM EDTA, 1% IGEPAL, 10% glycerol, 1 mM MgCl₂, 1 mM CaCl₂, and 150 mM NaCl for adipose tissue and a modified RIPA buffer containing 50 mM Tris-HCl, 150 mM NaCl, 1% IGEPAL, and 0.25% 1 mM EDTA for THP-1 cells; both were supplemented with protease and phosphatase inhibitors from Roche Diagnostics

(Complete Mini and PhosSTOP cocktails, respectively). Homogenates were incubated on ice for 10 min and centrifuged at $14,000 \times g$, 15 min (cells) or $16,000 \times g$, 40 min (tissue) at 4°C. Total protein (30–40 μ g) from supernatants was placed in SDS-containing Laemmli sample buffer, heated for 5 min at 95°C, and separated by 12% SDS-PAGE for 120 min at 120 V. Transfer was performed using the iBlot Dry Blotting System (Invitrogen) onto polyvinylidene difluoride membranes at 20 V over 7 min, and the efficiency of the transfer was visualized by Ponceau S staining. The membranes were soaked for 1 h at room temperature in 0.1% TBST and 5% (w/v) nonfat dry milk. Blots were washed three times, for 5 min each, with 0.1% TBST and incubated overnight at 4°C with primary anti-human Abs for HO-1, SOCS3, phospho-STAT1 (Tyr⁷⁰¹), phospho-STAT3 (Tyr⁷⁰⁵), phospho-p38 MAPK (Thr¹⁸⁰/Tyr¹⁸²), STAT1, STAT3, and p38 MAPK (all from Cell Signaling Technology). Thereafter, the blots were washed three times, for 5 min each, with 0.1% TBST containing 5% (w/v) nonfat dry milk and incubated for 1 h at room temperature with donkey anti-rabbit (BioLegend) or anti-mouse (Cell Signaling Technology) HRP-linked Ab (1:2000) in 0.1% TBST. Bands were visualized using the EZ-ECL Chemiluminescence Detection Kit (Biological Industries). To assess housekeeping protein expression, membranes were reblotted overnight at 4°C with primary rabbit anti-human GAPDH Ab (Imgenex) or β -actin HRP conjugate (Cell Signaling Technology) and detected and visualized as described above. Total STAT1, STAT3, p38 MAPK, GAPDH, or β -actin was used as an internal CT to verify basal expression levels and equal protein loading.

High-throughput transcriptomic analysis

RNA profiling was conducted in adipose tissue samples from four patients with morbid obesity and four CT subjects using the Affymetrix Human Genome U219 Array Plate containing >36,000 transcripts and variants. Preparation of complementary RNA probes, hybridization, and scanning of arrays were performed according to the manufacturer's protocol and carried out by the Functional Genomics Unit of August Pi i Sunyer Biomedical Research Institute. Affymetrix gene-expression data were normalized with the robust multiarray algorithm using a custom probe set definition that maps probes directly to Entrez Gene Ids (HGU219_Hs_ENTREZG). A filtering step excluding probes not reaching a coefficient of variation of 0.02 was used, and the total number of obtained probes was 13,928. For the detection of differentially expressed genes, a linear model was fitted to the data, and empirical Bayes moderated statistics were calculated using the limma package (Bioconductor). Adjustment of p values was done by the

FIGURE 4. RvD1 modulates IL-10-induced STAT3 activation. **(A)** Representative immunoblot of STAT3 and pSTAT3^{Tyr}, as assessed by Western blot in visceral adipose tissue samples from CT ($n = 8$) and Ob ($n = 14$) individuals. The densitometric analysis of pSTAT3^{Tyr}/STAT3 is shown on the right. **(B)** Representative immunoblots of pSTAT3^{Tyr} and total STAT3 levels in adipose tissue explants incubated with increasing concentrations of RvD1 (0, 1, 10, and 50 nM) for 30 min, followed by the addition of IL-10 (20 ng/ml) for 30 or 120 min. **(C)** Kinetic analysis of pSTAT3^{Tyr} in adipose tissue explants incubated in the absence (●) or presence (○) of RvD1 and stimulated with IL-10. **(D)** Representative immunoblots of STAT3 activation in THP-1 monocytes incubated in the presence of increasing concentrations of IL-10 for 10 min (upper panel). Densitometric analysis of phosphorylated protein/total protein (lower panel). **(E)** Representative immunoblots of STAT3 and pSTAT3^{Tyr} in THP-1-derived macrophages incubated in the presence of increasing concentrations of RvD1 for 30 min, followed by the addition of IL-10 (20 ng/ml) for 10 min (upper panel). Densitometric analysis of phosphorylated protein/total protein (lower panel). Data are mean \pm SEM of $n = 3$ independent experiments performed in duplicate. * $p < 0.05$ versus vehicle (0.01% ethanol) at time 0. ^a $p < 0.05$, ^b $p < 0.01$, RvD1 versus vehicle at 120 min.



determination of false discovery rates using the Benjamini–Hochberg procedure (17). All computations were done using R statistical software. Genes with a fold change ≥ 1.5 and a moderated p value < 0.05 were considered differentially expressed. Microarray data were submitted to the Gene Expression Omnibus under accession number GSE71415 (<http://www.ncbi.nlm.nih.gov/genbank>).

Metabololipidomics using liquid chromatography–tandem mass spectrometry

Adipose tissues were suspended in 1 ml of cold methanol, gently homogenized, and kept on ice for 1 h to allow for protein precipitation. Lipid mediators were profiled as described (18). Briefly, lipid mediators were extracted by solid-phase extraction using C18 columns and eluted using methyl formate. Fractions were subjected to liquid chromatography–tandem mass spectrometry (LC-MS/MS)–based lipidomics using a QTRAP 6500 (AB Sciex) mass spectrometer coupled to a Shimadzu HPLC system. Calibration curves were obtained using synthetic and authentic lipid mediator mixtures. Linear calibration curves for each were obtained with r^2 values in the range of +0.98 to +0.99. Quantification was carried out based on the peak area of the multiple reaction monitoring transition and the linear calibration curve for each compound or compounds with similar physical properties.

Luminex xMAP technology

Cytokine levels were determined in cell culture supernatants (25 μ l) using a multiplexed bead-based immunoassay (Milliplex MAP Human Cytokine/Chemokine Magnetic Bead Panel; Merck Millipore) on a Luminex 100 Bioanalyzer. The readouts were analyzed with the standard version of Milliplex Analyst software (Merck Millipore). A five-parameter logistic regression model was used to create standards curves (pg/ml) and to calculate the concentration of each sample.

Measurement of IL-10 levels

Levels of IL-10 in supernatants from adipose tissue explants were determined by a specific enzyme-linked immunoassay (Human IL-10 ELISA Kit; Invitrogen).

Statistical analysis of the results was performed using the unpaired Student t test. For multivariate statistical analysis, partial least squares–discriminant analysis (PLS-DA) was performed using SIMCA 13.0.3 software (Umetrics) following mean centering and unit variance scaling of lipid mediator amounts. Results are expressed as mean \pm SEM, and differences were considered significant at p values ≤ 0.05 .

Results

The demographic and clinical characteristics of the patients included in the study are shown in Supplemental Table I. Ob individuals had increased body weight, BMI, and serum triglyceride levels and a higher incidence of hepatic steatosis (Supplemental Table I). There were no statistically significant differences in gender or levels of serum glucose, cholesterol, alanine aminotransferase, or aspartate aminotransferase between the two study cohorts. The Ob cohort was younger than the nonobese group (Supplemental Table I). As is typical of obesity, this cohort presented a greater incidence of type II diabetes and hypertension and took antihypertensive (β -blockers, ACE inhibitors, and angiotensin II receptor antagonists) and antidiabetic (metformin and glimepiride) drugs at higher frequency than the nonobese CT group.

We first performed gene-expression profiling by microarray analysis of omental adipose tissue from Ob (BMI > 29.9) and

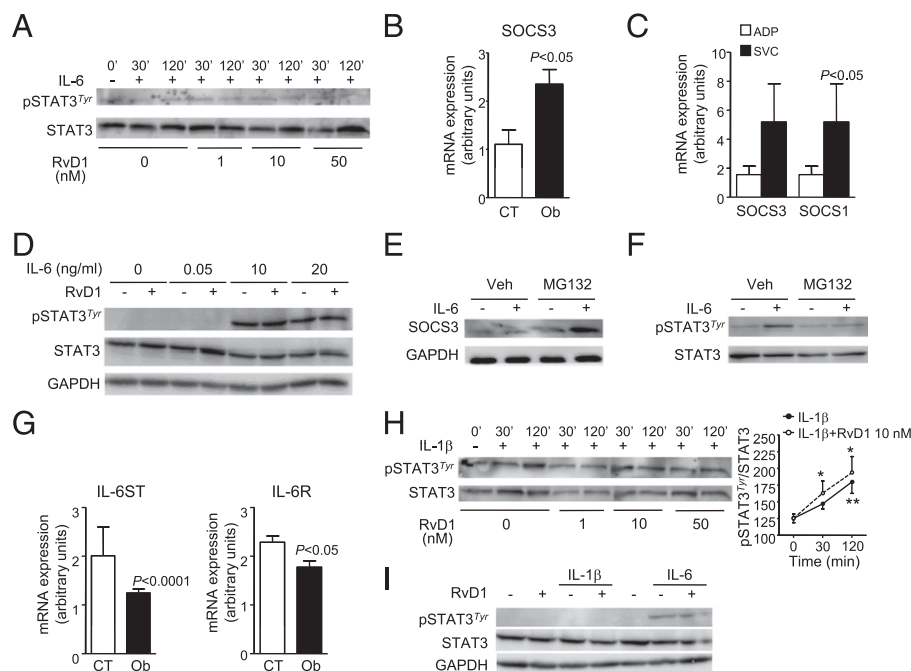


FIGURE 5. Ob adipose tissue explants are not responsive to IL-6–induced STAT3 phosphorylation. **(A)** Representative immunoblots of STAT3 and pSTAT3^{Tyr} assessed by Western blot in adipose tissue explants incubated with increasing concentrations of RvD1 (0, 1, 10, and 50 nM) for 30 min, followed by the addition of IL-6 (10 ng/ml) for 30 or 120 min. **(B)** SOCS3 mRNA expression in adipose tissue from CT ($n = 8$) and Ob ($n = 24$) individuals. **(C)** mRNA expression for SOCS3 and SOCS1 was analyzed in ADPs and SVCs isolated from human Ob adipose tissue. **(D)** Representative immunoblot of STAT3 and pSTAT3^{Tyr} in THP-1 monocytes incubated in the absence (–) or presence (+) of RvD1 (10 nM) for 30 min, followed by the addition of increasing concentrations of IL-6 for 10 min. **(E)** Representative immunoblots of SOCS3 and GAPDH in THP-1 cells incubated with vehicle (0.2% ethanol) or MG132 (10 μ M) for 30 min before the addition of IL-6 (10 ng/ml) for 5 h. **(F)** Representative immunoblots of STAT3 and pSTAT3^{Tyr} in THP-1 cells incubated with IL-10 (20 ng/ml) for 30 min before the addition of IL-6 (10 ng/ml) in the presence of vehicle (0.2% ethanol) or MG132 (10 nM) for 5 h. **(G)** Relative mRNA levels of IL-6 signal transducer (ST), also known as gp130, and IL-6R genes in human adipose tissue from CT ($n = 6$) and Ob ($n = 18$) subjects were assessed by real-time PCR relative to a calibrator sample consisting of total RNA derived from normal human adipose tissue pooled from 18 individuals. **(H)** Representative immunoblots of STAT3 activation assessed by Western blot in adipose tissue explants incubated with increasing concentrations of RvD1 (0, 1, 10, and 50 nM) for 30 min, followed by the addition of IL-1 β (25 pg/ml) for 30 or 120 min (left panel). Kinetic analysis of pSTAT3^{Tyr} in adipose tissue explants incubated in the absence (●) or presence (○) of RvD1 (10 nM) and stimulated with IL-1 β (right panel). **(I)** Representative immunoblots of STAT3 and pSTAT3^{Tyr} in THP-1–derived macrophages incubated in the absence (–) or presence (+) of RvD1 (10 nM) for 30 min, followed by the addition of IL-1 β (25 pg/ml) or IL-6 (10 ng/ml) for 10 min. Data are mean \pm SEM of $n = 3$ independent experiments performed in duplicate. * $p < 0.05$, ** $p < 0.005$ versus vehicle (0.01% ethanol) at time 0.

nonobese CT (BMI < 29.9) individuals. High-throughput transcriptome and subsequent functional analyses identified a group of genes associated with the inflammatory process that was differentially modulated in obesity (Fig. 1A). Among these, we found a significantly upregulated fold change in the expression of genes involved in IL-10 signaling, including IL-10 (1.77, $p < 0.0005$) and its receptor (IL-10RA) (1.5, $p < 0.05$), and downstream targets, such as HO-1 (2.23, $p < 0.05$) and CD163 (1.84, $p < 0.05$) (Fig. 1A). These changes were associated with a high inflammatory burden (i.e., overexpression of IL-6 and IL-1 β) in Ob adipose tissue (Fig. 1A). Overexpression of cytokines/adipokines was confirmed by real-time PCR (Fig. 1B). Cyclooxygenase-2 was also significantly upregulated in adipose tissue from Ob subjects (Supplemental Fig. 1A). Finally, compared with the CT group, omental adipose tissue from Ob patients showed an increased macrophage content, as revealed by CD68 immunostaining (Fig. 1C). Increased macrophage infiltration was confirmed by real-time PCR analysis of this macrophage marker, the expression of which increased gradually in a BMI-dependent manner (Fig. 1D).

We next profiled the levels of bioactive lipid mediators in visceral adipose tissue samples by LC-MS/MS-based metabololipidomics. Human visceral adipose tissue produced the full spectrum of SPMs derived from endogenous sources of docosahexaenoic acid (i.e., D-series resolvins, protectin D1 and maresin 1), eicosapentaenoic acid (i.e., E-series resolvins), and arachidonic acid (lipoxin [LX] A_4 and AT-LXA $_4$). These mediators were identified based on published criteria that include matching retention times (Fig. 2A) and at least six characteristic and diagnostic ions for each, as illustrated by the results obtained for RvD1 (Fig. 2B). Visceral adipose tissue also had detectable levels of arachidonic acid-derived 5-lipoxygenase products [i.e., leukotriene (LT) B_4 and its all-*trans* isomer 5(S),12(S)-dihydroxy-6,10-*trans*-8,14-*cis*-eicosatetraenoic acid], PGs (i.e., PGE $_2$, PGD $_2$, and PGF $_{2\alpha}$), and thromboxane A $_2$ (Fig. 2A). Quantitation of lipid mediators in Ob and nonobese adipose tissue is

given in Supplemental Table II. Notably, adipose tissue samples from Ob patients showed a reduced ratio between SPM levels and both 5-lipoxygenase products (i.e., LTB $_4$ and its all-*trans* isomer) and PGs (Fig. 2C). We used data-driven modeling to further interrogate the lipid mediator profiles obtained from Ob and nonobese adipose tissue. PLS-DA of lipid mediator profiles obtained from Ob patients gave a distinct cluster in principle component 1 (Fig. 2D, left panel). The loading plot demonstrated that proresolving mediators, including RvD1 and RvD5, as well as the inflammation-initiating eicosanoids LTB $_4$ and thromboxane B $_2$, associate with profiles obtained from Ob adipose tissues with variable importance in projection scores > 1, whereas RvD2 and RvD3 were associated with profiles from CT patients (Fig. 2D, right panel). Interestingly, multiple linear regression analysis identified a close relationship between SPM and IL-10 and between IL-10 and CD68 in adipose tissue (Fig. 2E). SPM levels did not correlate with IL-1 β and IL-6 (Supplemental Fig. 1B). In contrast, tissue levels of LTB $_4$ and its all-*trans* isomer correlated with IL-10 and IL-1 β expression (Supplemental Fig. 1C), whereas levels of PGs correlated only with IL-10 (Supplemental Fig. 1D).

To understand how cytokines/adipokines influence adipose tissue inflammation and how this can be modulated by SPMs, we next performed ex vivo experiments in adipose tissue explants from Ob patients. As shown in Fig. 3A, addition of recombinant human IL-10 to fat explants exerted anti-inflammatory properties by decreasing the expression of IL-6, IL-1 β , IL-8, and TNF- α . Addition of IL-1 β produced the opposite effect and induced the expression of inflammatory cytokines/adipokines (Fig. 3B). In contrast, Ob adipose tissue was not responsive to IL-6 stimulation (Fig. 3C). IL-10 enhanced its own expression in adipose tissue in a statistically significant manner (Fig. 3D), whereas this autoregulatory loop was not seen with IL-1 β and IL-6 (data not shown). The IL-10 positive-feedback loop was also present in human THP-1 macrophages (Fig. 3E). These cells were selected because they

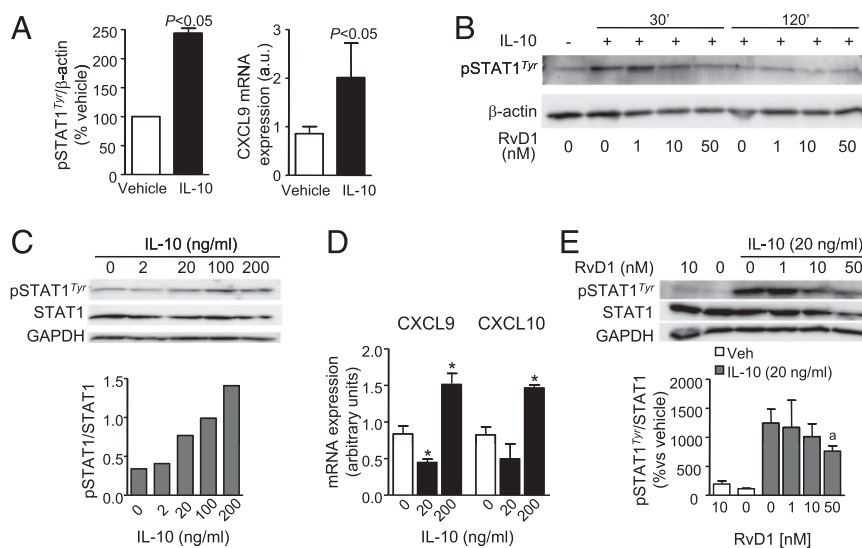


FIGURE 6. RvD1 attenuates IL-10-induced STAT1 activation in human Ob adipose tissue and macrophages. **(A)** Levels of STAT1 Tyr⁷⁰¹ phosphorylation (pSTAT1^{Tyr}) after 30 min of IL-10 stimulation and expression of its target gene CXCL9 in Ob adipose tissue explants incubated for 6 h with IL-10 (20 ng/ml). **(B)** Representative immunoblots of pSTAT1^{Tyr} and β-actin assessed by Western blot in visceral adipose tissue explants incubated with increasing concentrations of RvD1 (0, 1, 10, and 50 nM) for 30 min, followed by the addition of IL-10 (20 ng/ml) for 30 or 120 min. **(C)** Representative immunoblots analyzing STAT1 activation in THP-1 monocytes incubated in the presence of increasing concentrations of IL-10 for 10 min (upper panel). Densitometric analysis of phosphorylated protein/total protein (lower panel). **(D)** mRNA expression for STAT1 target genes (CXCL9 and CXCL10) in THP-1-derived macrophages incubated in the presence of increasing concentrations of IL-10 for 6 h. **(E)** Representative immunoblots of STAT1 and pSTAT1^{Tyr} in THP-1-derived macrophages incubated in the presence of increasing concentrations of RvD1 for 30 min, followed by the addition of IL-10 (20 ng/ml) for 10 min (upper panel). Densitometric analysis of phosphorylated protein/total protein (lower panel). Data are mean ± SEM of $n = 3$ independent experiments performed in duplicate. * $p < 0.05$ versus vehicle, ^a $p < 0.05$ versus IL-10-treated cells.

provide an optimal platform in which to perform mechanistic studies of one of the predominant immune cell types present in the SVC fraction of adipose tissue. Indeed, compared with ADPs, cells of the SVC fraction were the major contributors to cytokine/adipokine production in visceral fat from Ob individuals (Fig. 3F). Another observation from Ob fat explants is that IL-10 induced the expression of CD163 and HO-1, which are part of the IL-10-induced anti-inflammatory response (19) (Fig. 3G). HO-2 was also upregulated by IL-10 (Supplemental Fig. 2A). Moreover, the HO-1 mRNA response to IL-10 was amplified in adipose tissue explants from Ob patients incubated with 10 nM RvD1 (Fig. 3H). Similarly, RvD1 at 1 nM amplified, in an additive fashion, IL-10-induced HO-1 protein expression after 120 min of incubation (Fig. 3I). Unexpectedly, high concentrations of RvD1 (>10 nM) reduced HO-1 protein expression in adipose tissue explants (Fig. 3I). RvD1 did not modify CD163 expression in resting or IL-10-treated adipose tissue explants (Supplemental Fig. 2B). Strengthening of the IL-10-mediated HO-1 response induced by RvD1 was confirmed in human THP-1 macrophages (Fig. 3J).

To identify signaling events that may mediate RvD1 actions on the IL-10-induced anti-inflammatory response, we next investigated the canonical IL-10/STAT3 pathway in Ob adipose tissue. As shown in Fig. 4A, human adipose tissue showed a constitutive phosphorylation on the Tyr⁷⁰⁵ residue of STAT3, with the extent of phosphorylation being significantly higher in Ob individuals than

in nonobese CT subjects. Consistent with the fact that the IL-10 response is preserved in Ob adipose tissue, this cytokine activated STAT3^{Tyr} phosphorylation after 120 min of stimulation (Fig. 4B). Notably, pretreatment with RvD1 at 1 nM significantly sensitized adipose tissue to IL-10 and shifted the maximal induction of STAT3^{Tyr} phosphorylation to the left and upward at 30 min (Fig. 4C). In contrast, RvD1 significantly reduced IL-10-induced STAT3^{Tyr} phosphorylation at higher concentrations (10 and 50 nM) and for longer periods of time (120 min) (Fig. 4C). Importantly, the IL-10-induced anti-inflammatory response (characterized by inhibition of IL-6, IL-1 β , IL-8, and TNF- α) was preserved in adipose tissue during RvD1 treatment, and this SPM reduced IL-8 expression even further (Supplemental Fig. 2C). A concentration-dependent increase in STAT3^{Tyr} phosphorylation in response to IL-10 and its downregulation by RvD1 were confirmed in human THP-1 macrophages (Fig. 4D, 4E).

In addition to IL-10, cytokines such as IL-6 use receptor-induced signaling through the JAK/STAT3 pathway. Paradoxically, and in contrast to IL-10, IL-6 produces an opposed transcriptional and proinflammatory response (20). For this reason, we next explored whether RvD1 was able to modulate STAT3^{Tyr} phosphorylation of Ob fat explants exposed to IL-6. Consistent with Ob adipose tissue's lack of response to IL-6, this cytokine/adipokine was totally ineffective in inducing phosphorylation of STAT3^{Tyr} in this human tissue, a response that was not modified by RvD1 (Fig. 5A).

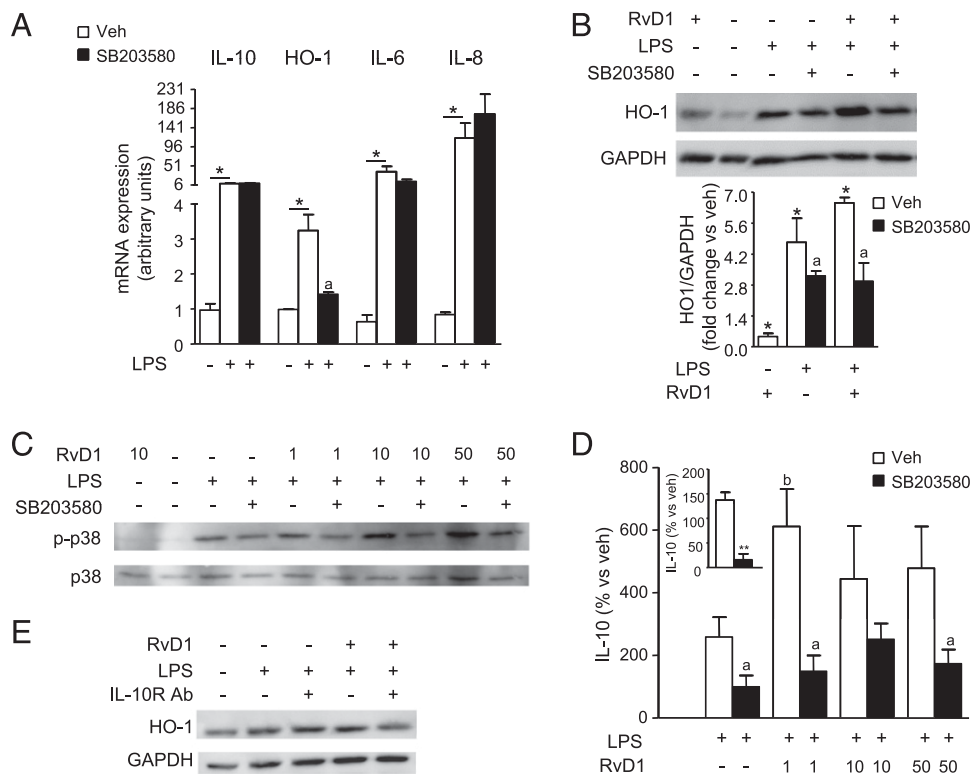


FIGURE 7. RvD1 enhances the production of HO-1 and IL-10 by a p38 MAPK-dependent mechanism in human monocytes. **(A)** mRNA expression for IL-10, HO-1, IL-6, and IL-8 in THP-1 cells incubated with the p38 MAPK inhibitor SB203580 (5 μ M) for 30 min before the addition of LPS (1 μ g/ml) for 6 h. **(B)** Representative immunoblot (upper panel) and densitometric analysis (lower panel) of HO-1 protein expression in THP-1 cells incubated with RvD1 (10 nM) in the presence or absence of SB203580 (5 μ M) for 30 min before the addition of LPS (1 μ g/ml) for 6 h. **(C)** Representative immunoblots of p38 MAPK and its phosphorylated form (p-p38, phosphorylation at Thr¹⁸⁰/Tyr¹⁸²) in THP-1 cells incubated with RvD1 (1, 10, and 50 nM) and SB203580 (5 μ M) for 30 min before the addition of LPS (1 μ g/ml) for 6 h. **(D)** IL-10 levels in supernatants of cultured human Ob adipose tissue explants incubated with the p38 MAPK inhibitor SB203580 (5 μ M) in the presence of increasing concentrations of RvD1 for 30 min before the addition of LPS (1 μ g/ml) for 24 h were detected by a specific ELISA kit (see *Materials and Methods* for details). Basal IL-10 levels in untreated (open bar) and RvD1 (10 nM)-treated cells (filled bar) are shown (inset). Protein levels are shown as the percentage of IL-10 production relative to untreated tissue explants. **(E)** Representative immunoblot of HO-1 in THP-1 cells incubated with RvD1 (10 nM) for 30 min before the addition of LPS (1 μ g/ml) in the presence or absence of a neutralizing Ab to IL-10R (10 μ g/ml) for 6 h. Data are mean \pm SEM. * p < 0.05 versus LPS-untreated cells, ** p < 0.005 versus vehicle, ^a p < 0.05 versus its paired LPS-stimulated cells without SB203580 pretreatment, ^b p < 0.05 versus LPS-treated cells.

Because, in contrast to IL-10, STAT3 activation by IL-6 is negatively regulated by SOCS3, a member of the family of SH2-containing E3 ligases (21), this lack of effectiveness could be related to the observed upregulation of SOCS3 in Ob adipose tissue (Fig. 5B). Similar upregulation was detected in the high-throughput transcriptome analysis (5.3-fold increase in Ob versus CT nonobese, $p < 0.05$). Moreover, multiple linear regression identified a close direct relationship between SOCS3 and IL-6 in human adipose tissue (Supplemental Fig. 2D). Given that SOCS3 and SOCS1 are predominantly expressed in the SVC fraction of visceral adipose tissue from Ob individuals (Fig. 5C), we performed mechanistic studies in human THP-1 cells. In these cells, and in contrast to what was observed in Ob adipose tissue, IL-6 produced the expected induction in STAT3^{Tyr} phosphorylation (Fig. 5D). As a proof of concept that SOCS3 is involved in the blunted response to IL-6, we obtained data showing that this canonical response of IL-6 signaling disappears in the presence of MG132, a proteasome inhibitor that has the ability to stabilize SOCS3 in response to IL-6 (Fig. 5E, 5F). Nevertheless, the unresponsiveness of Ob adipose tissue to IL-6 could be multifactorial and depend on different mechanisms because, for instance, the expression of IL-6R and its transactivator gp130 is significantly downregulated in visceral adipose tissue from Ob individuals (Fig. 5G). Recent studies suggested that, in addition to IL-10 and IL-6, the STAT3 pathway is part of the noncanonical IL-1 β signaling pathway (22, 23). IL-1 β was also able to induce STAT3^{Tyr} phosphorylation after 30 min of incubation in visceral Ob adipose tissue but not in THP-1 cells; these responses were not modified significantly by RvD1 (Fig. 5H, 5I).

Excessive overactivation of the IL-10 signaling pathway during type I IFN-derived responses can lead to the undesired activation of STAT1 and its target inflammatory genes (i.e., CXCL9) (24). As shown in Fig. 6A, significant phosphorylation of STAT1^{Tyr} and induction of CXCL9 were observed after incubating Ob adipose tissue with IL-10. Importantly, this IL-10-induced STAT1^{Tyr} phosphorylation signal was repressed by RvD1 (Fig. 6B). Overstimulation of the STAT1^{Tyr} pathway by IL-10 also was observed in THP-1 cells incubated with high concentrations (>100 ng/ml) of this cytokine (Fig. 6C). Consistently, the expression of STAT1-dependent genes (i.e., CXCL9 and CXCL10) was upregulated by high concentrations of IL-10 (Fig. 6D). Similar to the observations in Ob adipose tissue, RvD1 attenuated IL-10-induced STAT1^{Tyr} phosphorylation in these cells in a concentration-dependent manner (Fig. 6E).

The STAT3 signaling pathway is necessary, but not sufficient, for the IL-10 anti-inflammatory response; for instance, this cytokine can induce HO-1 expression in LPS-elicited macrophages via a p38 MAPK pathway (25, 26). In view of this, we next investigated the impact of RvD1 on the anti-inflammatory production of IL-10 in response to LPS. As shown in Fig. 7A, LPS significantly upregulated IL-10, HO-1, IL-6, and IL-8 expression. Of note, LPS-mediated HO-1 induction was blocked by the selective p38 MAPK inhibitor SB203580, confirming that the p38 MAPK signaling pathway is involved in the production of HO-1 (Fig. 7A). Under these inflammatory conditions, RvD1 induced a further upregulation of HO-1, an effect that also was dependent on p38 MAPK signaling (Fig. 7B). Consistent with this finding, RvD1 increased the phosphorylation of p38 MAPK in a concentration-dependent manner; this also was blocked by the selective p38 MAPK inhibitor SB203580 (Fig. 7C). In parallel with this, RvD1 enhanced IL-10 production (Fig. 7D), suggesting that this SPM modulates HO-1 in an IL-10-dependent manner. Consistently, induction of HO-1 by RvD1 was partially blocked by a selective Ab directed against IL-10R (Fig. 7E). Interestingly, measurement of cytokine levels in cell supernatants from these experiments in a multiplex assay revealed that RvD1 is also able to increase, in a

concentration-dependent manner, the secretion of IL-1 β receptor antagonist (IL-1ra), a natural inhibitor of the proinflammatory actions of IL-1 β (27) (Supplemental Fig. 2E). The induction of IL-1ra release by RvD1 was also dependent on p38 MAPK activity (Supplemental Fig. 2E). A schematic diagram summarizing RvD1 actions on the IL-10 signaling pathway is shown in Fig. 8.

Discussion

The results of this study advance the concept that SPMs promote resolution and actively suppress uncontrolled inflammation in adipose tissue from Ob individuals. In particular, the proresolving actions of RvD1 in this tissue are mediated through its interaction with the pathways signaling for IL-10 and through the modulation of the archetypal anti-inflammatory response of this cytokine. The current findings add to previous work in preclinical models of obesity showing that RvD1 and other SPMs attenuate adipose tissue inflammation by reducing the production of cytokines/adipokines (i.e., TNF- α , IL-6, and MCP-1) and shifting the phenotype of recruited macrophages toward the M2 proresolving state (8, 10–12). Accordingly, the most innovative aspect of the current study is the translation of these therapeutic benefits to the clinical scenario, as our results have been obtained in samples of adipose tissue from Ob individuals.

Visceral adipose tissue from Ob patients showed exaggerated expression of inflammatory and anti-inflammatory cytokines/adipokines. Additionally, it exhibited increased levels of inflammatory (LTs and PGs) and anti-inflammatory/proresolving (SPM) lipid mediators. However, the ratio between SPM levels and both LTs and PGs production was reduced significantly in adipose tissue samples from Ob individuals. This observation indicates the presence of a notable deficit in SPM levels compared with proinflammatory signals and the impaired ability of visceral adi-

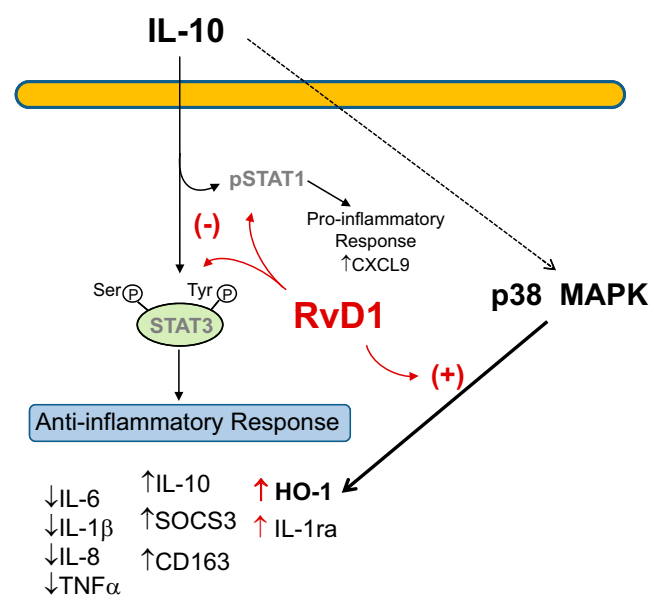


FIGURE 8. Schematic diagram of the interaction of RvD1 with the IL-10 signaling pathway. IL-10 promotes a STAT3-mediated anti-inflammatory response characterized by reduced expression of proinflammatory cytokines and increased expression of anti-inflammatory targets. Persistent activation of STAT signaling by IL-10 results in a proinflammatory response characterized by the upregulation of the STAT1-dependent CXCL9 target. In these conditions, RvD1 limits excessive overactivation of the STAT pathway while maintaining the IL-10-induced anti-inflammatory response via positive regulation of HO-1 through the p38 MAPK pathway. The p38 MAPK pathway also signals the actions of RvD1 on IL-1ra, a natural inhibitor of the proinflammatory actions of IL-1 β .

pose tissue to resolve uncontrolled inflammation in this condition. These findings are in agreement with those reported in other fat depots, such as s.c. and perivascular fat from patients with metabolic syndrome (28). Because visceral adipose is recognized to be central to metabolic diseases and to have a more negative impact on health than other fat depots (29), our data support the concept that persistent unresolved inflammation in adipose tissue is one of the most important factors driving the metabolic complications associated with obesity, including insulin resistance and NAFLD (1, 2).

Visceral adipose tissue from Ob individuals appears to display a characteristic response to the actions of cytokines/adipokines. For example, Ob adipose tissue remains sensitive to the inflammatory actions of IL-1 β . Similarly, the anti-inflammatory response elicited by IL-10, which is characterized by inhibition of inflammatory cytokines/adipokines, such as IL-6, IL-1 β , IL-8, and TNF- α , is preserved in this tissue. In sharp contrast, Ob adipose tissue is unresponsive to IL-6; moreover, the signal-transduction pathways activated by these cytokines/adipokines display a disorganized pattern. For example, STATs are the classical transcription factors transducing the signals elicited by type I and type II cytokine receptors (30). In the case of IL-10, binding of this cytokine to its receptor activates JAK, which is associated with the cytoplasmic domain of the receptor. The activated receptor-JAK complex then recruits and promotes Tyr⁷⁰⁵ phosphorylation of STAT3 (pSTAT3^{Tyr}) proteins, leading to their homodimerization and subsequent translocation to the nucleus where phosphorylated STAT3 dimers bind to STAT3-binding elements of IL-10-responsive genes (31). The results of the current study support the concept that STAT3 is required, but not sufficient, for mediating IL-10-induced anti-inflammatory responses in inflamed Ob adipose tissue. In this regard, our findings reveal that the p38 MAPK signaling pathway is involved in the regulation of HO-1 expression. This is in agreement with previous studies proposing p38 MAPK as the pathway signaling the anti-inflammatory responses to IL-10 in murine macrophages (32). Moreover, our findings identify the p38 MAPK signaling pathway as a genuine mechanism underlying the additive anti-inflammatory actions of RvD1 and IL-10 in Ob adipose tissue. This observation is in agreement with that reported by Cooray et al. (33), establishing that phosphorylation of p38 MAPK is engaged in the proresolving signature of ALX activation, the receptor mediating the actions of other SPMs, such as LXA₄ and annexin A1. Another example of the peculiarities of Ob adipose tissue in terms of activation of signal-transduction pathways by cytokines/adipokines is that incubation of fat explants with rIL-1 β resulted in the phosphorylation of STAT3, an effect that was not modulated by RvD1. Although other investigators demonstrated the activation of STAT3 in response to IL-1 β (22, 23), unlike IL-10 and IL-6, this is a noncanonical pathway for IL-1 β signaling. Finally, the observation that high concentrations of IL-10 induce STAT1 phosphorylation in Ob adipose tissue deserves some comment. This is not surprising because excessive overactivation of the IL-10 signaling pathway during type I IFN-derived responses can lead to undesired activation of STAT1 and its target inflammatory genes (i.e., CXCL9 and CXCL10) (24). Of paramount importance is the fact that this IL-10-induced STAT1 phosphorylation is significantly repressed by RvD1, which indicates that, in addition to promoting IL-10 anti-inflammatory responses, RvD1 plays a role as a braking signal that limits excessive overactivation of the IL-10 signaling pathways. Fig. 8 summarizes most of the actions elicited by IL-10 in Ob adipose tissue and the modulation by RvD1.

In summary, our study describes novel signal-regulatory mechanisms for RvD1 that culminate in the promotion of a more intense IL-10-induced anti-inflammatory response in inflamed human ad-

ipose tissue. These findings are in accordance with previous studies in other organs, tissues, and cells in which RvD1 counterregulates inflammatory signals while promoting the secretion of anti-inflammatory cytokines (34), thus highlighting the proresolving functions of these lipid mediators.

Acknowledgments

We thank the surgical and nursing staff from the Department of Gastrointestinal Surgery and the Ambulatory Surgery Unit, Hospital Clínic, for their professionalism and dedication in providing human samples. We also thank Dr. Romain Colas, Brigham and Women's Hospital-Harvard Medical School, for expert help with validation of SPM physical properties and LC-MS/MS profiling, and Ana Isabel Martínez-Puchol, Department of Biochemistry and Molecular Genetics, Hospital Clínic, for her technical assistance.

Disclosures

C.N.S. is an inventor on several patents (resolvins) assigned to Brigham and Women's Hospital and licensed to Resolvix Pharmaceuticals, a scientific founder of Resolvix Pharmaceuticals with equity ownership in the company, and has interests reviewed and managed by the Brigham and Women's Hospital and Partners HealthCare in accordance with their conflict of interest policies. The other authors have no financial conflicts of interest.

References

- Ferrante Jr., A. W., 2007. Obesity-induced inflammation: a metabolic dialogue in the language of inflammation. *J. Intern. Med.* 262: 408–414.
- Hotamisligil, G. S., 2006. Inflammation and metabolic disorders. *Nature* 444: 860–867.
- Ouchi, N., J. L. Parker, J. J. Lugus, and K. Walsh., 2011. Adipokines in inflammation and metabolic disease. *Nat. Rev. Immunol.* 11: 85–97.
- Chawla, A., K. D. Nguyen, and Y. P. Goh., 2011. Macrophage-mediated inflammation in metabolic disease. *Nat. Rev. Immunol.* 11: 738–749.
- Spite, M., J. Clària, and C. N. Serhan., 2014. Resolvins, specialized proresolving lipid mediators, and their potential roles in metabolic diseases. *Cell Metab.* 19: 21–36.
- Gilroy, D. W., T. Lawrence, M. Perretti, and A. G. Rossi., 2004. Inflammatory resolution: new opportunities for drug discovery. *Nat. Rev. Drug Discov.* 3: 401–416.
- Serhan, C. N., 2014. Pro-resolving lipid mediators are leads for resolution physiology. *Nature* 510: 92–101.
- Hellmann, J., Y. Tang, M. Kosuri, A. Bhatnagar, and M. Spite., 2011. Resolvin D1 decreases adipose tissue macrophage accumulation and improves insulin sensitivity in obese-diabetic mice. *FASEB J.* 25: 2399–2407.
- González-Pérez, A., R. Horrillo, N. Ferré, K. Gronert, B. Dong, E. Morán-Salvador, E. Títos, M. Martínez-Clemente, M. López-Parra, et al., 2009. Obesity-induced insulin resistance and hepatic steatosis are alleviated by omega-3 fatty acids: a role for resolvins and protectins. *FASEB J.* 23: 1946–1957.
- Títos, E., B. Rius, A. González-Pérez, C. López-Vicario, E. Morán-Salvador, M. Martínez-Clemente, V. Arroyo, and J. Clària., 2011. Resolvin D1 and its precursor docosahexaenoic acid promote resolution of adipose tissue inflammation by eliciting macrophage polarization toward an M2-like phenotype. *J. Immunol.* 187: 5408–5418.
- Clària, J., J. Dalli, S. Yacoubian, F. Gao, and C. N. Serhan., 2012. Resolvin D1 and resolvin D2 govern local inflammatory tone in obese fat. *J. Immunol.* 189: 2597–2605.
- Rius, B., E. Títos, E. Morán-Salvador, C. López-Vicario, V. García-Alonso, A. González-Pérez, V. Arroyo, and J. Clària., 2014. Resolvin D1 primes the resolution process initiated by calorie restriction in obesity-induced steatohepatitis. *FASEB J.* 28: 836–848.
- Schif-Zuck, S., N. Gross, S. Assi, R. Rostoker, C. N. Serhan, and A. Ariel., 2011. Saturated-efferocytosis generates pro-resolving CD11b low macrophages: modulation by resolvins and glucocorticoids. *Eur. J. Immunol.* 41: 366–379.
- Serhan, C. N., and J. Savill., 2005. Resolution of inflammation: the beginning programs the end. *Nat. Immunol.* 6: 1191–1197.
- Schwab, J. M., N. Chiang, M. Arita, and C. N. Serhan., 2007. Resolvin E1 and protectin D1 activate inflammation-resolution programmes. *Nature* 447: 869–874.
- Wiejak, J., J. Dunlop, S. P. Mackay, and S. J. Yarwood., 2013. Flavanoids induce expression of the suppressor of cytokine signalling 3 (SOCS3) gene and suppress IL-6-activated signal transducer and activator of transcription 3 (STAT3) activation in vascular endothelial cells. *Biochem. J.* 454: 283–293.
- Ritchie, M. E., B. Phipson, D. Wu, Y. Hu, C. W. Law, W. Shi, and G. K. Smyth., 2015. limma powers differential expression analyses for RNA-sequencing and microarray studies. *Nucleic Acids Res.* 43: e47.
- Colas, R. A., M. Shinohara, J. Dalli, N. Chiang, and C. N. Serhan., 2014. Identification and signature profiles for pro-resolving and inflammatory lipid mediators in human tissue. *Am. J. Physiol. Cell Physiol.* 307: C39–C54.
- Abraham, N. G., and G. Drummond., 2006. CD163-Mediated hemoglobin-heme uptake activates macrophage HO-1, providing an antiinflammatory function. *Circ. Res.* 99: 911–914.

20. El Kasmi, K. C., J. Holst, M. Coffre, L. Mielke, A. de Pauw, N. Lhocine, A. M. Smith, R. Rutschman, D. Kaushal, Y. Shen, et al. 2006. General nature of the STAT3-activated anti-inflammatory response. *J. Immunol.* 177: 7880–7888.
21. Yoshimura, A., T. Naka, and M. Kubo. 2007. SOCS proteins, cytokine signalling and immune regulation. *Nat. Rev. Immunol.* 7: 454–465.
22. Radtke, S., S. Wüller, X. P. Yang, B. E. Lippok, B. Mütze, C. Mais, H. S. de Leur, J. G. Bode, M. Gaestel, P. C. Heinrich, et al. 2010. Cross-regulation of cytokine signalling: pro-inflammatory cytokines restrict IL-6 signalling through receptor internalisation and degradation. *J. Cell Sci.* 123: 947–959.
23. Mori, T., T. Miyamoto, H. Yoshida, M. Asakawa, M. Kawasumi, T. Kobayashi, H. Morioka, K. Chiba, Y. Toyama, and A. Yoshimura. 2011. IL-1 β and TNF α -initiated IL-6-STAT3 pathway is critical in mediating inflammatory cytokines and RANKL expression in inflammatory arthritis. *Int. Immunol.* 23: 701–712.
24. Pike, K. A., A. P. Hutchins, V. Vinette, J. F. Théberge, L. Sabbagh, M. L. Tremblay, and D. Miranda-Saavedra. 2014. Protein tyrosine phosphatase 1B is a regulator of the interleukin-10-induced transcriptional program in macrophages. *Sci. Signal.* 7: ra43.
25. O'Farrell, A. M., Y. Liu, K. W. Moore, and A. L. Mui. 1998. IL-10 inhibits macrophage activation and proliferation by distinct signaling mechanisms: evidence for Stat3-dependent and -independent pathways. *EMBO J.* 17: 1006–1018.
26. Lee, T. S., and L. Y. Chau. 2002. Heme oxygenase-1 mediates the anti-inflammatory effect of interleukin-10 in mice. *Nat. Med.* 8: 240–246.
27. Arend, W. P., M. Malyak, C. J. Guthridge, and C. Gabay. 1998. Interleukin-1 receptor antagonist: role in biology. *Annu. Rev. Immunol.* 16: 27–55.
28. Clària, J., B. T. Nguyen, A. L. Madenci, C. K. Ozaki, and C. N. Serhan. 2013. Diversity of lipid mediators in human adipose tissue depots. *Am. J. Physiol. Cell Physiol.* 304: C1141–C1149.
29. Wajchenberg, B. L., D. Giannella-Neto, M. E. da Silva, and R. F. Santos. 2002. Depot-specific hormonal characteristics of subcutaneous and visceral adipose tissue and their relation to the metabolic syndrome. *Horm. Metab. Res.* 34: 616–621.
30. Schindler, C., D. E. Levy, and T. Decker. 2007. JAK-STAT signaling: from interferons to cytokines. *J. Biol. Chem.* 282: 20059–20063.
31. Villarino, A. V., Y. Kanno, J. R. Ferdinand, and J. J. O'Shea. 2015. Mechanisms of Jak/STAT signaling in immunity and disease. *J. Immunol.* 194: 21–27.
32. Ashwell, J. D. 2006. The many paths to p38 mitogen-activated protein kinase activation in the immune system. *Nat. Rev. Immunol.* 6: 532–540.
33. Cooray, S. N., T. Gobbetti, T. Montero-Melendez, S. McArthur, D. Thompson, A. J. Clark, R. J. Flower, and M. Perretti. 2013. Ligand-specific conformational change of the G-protein-coupled receptor ALX/FPR2 determines proresolving functional responses. *Proc. Natl. Acad. Sci. USA* 110: 18232–18237.
34. Croasdell, A., T. H. Thatcher, R. M. Kottmann, R. A. Colas, J. Dalli, C. N. Serhan, P. J. Sime, and R. P. Phipps. 2015. Resolvins attenuate inflammation and promote resolution in cigarette smoke-exposed human macrophages. *Am. J. Physiol. Lung Cell. Mol. Physiol.* 309: L888–L901.